J|A|C|S
ARTICLES

Size-Dependent Hydrogen Sorption in Ultrasmall Pd Clusters Embedded in a Mesoporous Carbon Template

Claudia Zlotea,*,† Fermin Cuevas,† Valérie Paul-Boncour,† Eric Leroy,†
Philippe Dibandjo,‡ Roger Gadiou,‡ Cathie Vix-Guterl,‡ and Michel Latroche†

Institut de Chimie et des Matériaux Paris Est (ICMPE), UMR 7182, CNRS, Thiais, France, and
Institut de Science des Matériaux de Mulhouse (IS2M), LRC 7227, CNRS, Mulhouse, France

Received March 3, 2010; E-mail: claudia.zlotea@icmpe.cnrs.fr

Abstract: Hydrogen sorption properties of ultrasmall Pd nanoparticles (2.5 nm) embedded in a mesoporous carbon template have been determined and compared to those of the bulk system. Downsizing the Pd particle size introduces significant modifications of the hydrogen sorption properties. The total amount of stored hydrogen is decreased compared to bulk Pd. The hydrogenation of Pd nanoparticles induces a phase transformation from fcc to icosahedral structure, as proven by in situ XRD and EXAFS measurements. This phase transition is not encountered in bulk because the 5-fold symmetry is nontranslational. The kinetics of desorption from hydrogenated Pd nanoparticles is faster than that of bulk, as demonstrated by TDS investigations. Moreover, the presence of Pd nanoparticles embedded in CT strongly affects the desorption from physisorbed hydrogen, which occurs at higher temperature in the hybrid material compared to the pristine carbon template.

Introduction

The downscaling and control of the metal particle sizes have become an important issue for the design of new solid-state hydrogen storage materials.[1−4] Downsizing the metal particles to few nanometers can introduce fundamental changes compared to the corresponding bulk state and therefore may overcome the drawbacks encountered in the latter materials. For small particles the ratio of surface to bulk atoms becomes important and surface effects may influence the total energy and modify the fundamental properties such as thermodynamics and kinetics of the hydrogen−metal interactions. Materials with small crystal and particle size have improved kinetics of hydrogen sorption.[3] Previously, theoretical calculations have proven that the thermodynamic properties of the Mg hydride can be destabilized when the metal clusters become smaller than 1.3 nm.[4]

Another important aspect of downsizing the metal particle size is related to their crystalline structure. Below a critical size for fcc metal clusters, a complete rearrangement of atoms may occur into new structures (icosahedral, dodecahedral) that possess crystal symmetry properties completely different from those of the bulklike systems.[5,6] Both icosahedral and dodecahedral structures have a 5-fold axis of rotation that is a nontranslational symmetry.

A major problem for the study and the use of nanosized particles is related to the instability at high temperature and the tendency for coalescence into larger aggregates. Different types of stabilizers (electrostatic or steric) are currently used to overcome this drawback.[7] Another possible solution is to embed metal clusters into the porosity of an ordered porous material with controlled pore size distribution. The well-defined pore dimension controls the dispersion of the clusters size distribution. The resulting material is a hybrid that combines the properties of each component: the metal nanoparticles and the porous structure. The advantage of this hybrid material as a hydrogen store medium is the combined gas sorption: *adsorption* on the surface of the pores of the porous material and *hydrogenation* of the metal clusters by forming hydrides. Moreover, the presence of metal clusters inside the pores is considered to increase the hydrogen uptake of different porous materials via the spillover effect (catalyzed formation of monatomic hydrogen followed by migration to the surface of the support).[8]

In the present work, hydrogen sorption properties of a hybrid material formed by Pd nanoparticles embedded into an ordered mesoporous carbon material are reported and discussed. The precursor and the hybrid material have been synthesized following already published methods.[9−14] The structural, microstructural, and textural properties of the carbon precursor and the hybrid material have been determined. In situ X-ray, neutron

---

† Institut de Chimie et des Matériaux Paris Est (ICMPE).
‡ Institut de Science des Matériaux de Mulhouse (IS2M).

(1) Dornheim, M.; Eigen, N.; Barkhordarian, G.; Klassen, T.; Bormann, R. *Adv. Eng. Mater.* **2006**, *8*, 377.
(2) Fichtner, M. *Nanotechnology* **2009**, *20*, 204009.
(3) Zaluska, A.; Zaluski, L.; Ström-Olsen, J. O. *J. Alloys Compd.* **1999**, *288*, 217.
(4) Wagemans, R. W. P.; van Lenthe, J. H.; de Jongh, P. E.; van Dillen, A. J.; de Jong, K. P. *J. Am. Chem. Soc.* **2005**, *127*, 16675.
(5) Reinhard, D.; Hall, B. D.; Berthoud, P.; Valkealahti, S.; Monot, R. *Phys. Rev. Lett.* **1997**, *79*, 1459.
(6) Marks, L. D. *Rep. Prog. Phys.* **1994**, *57*, 603.
(7) Ott, L. S.; Finke, R. G. *Coord. Chem. Rev.* **2007**, 1075.
(8) Wang, L.; Yang, R. T. *Energy Environ. Sci.* **2008**, *1*, 268.
(9) Ryoo, R.; Joo, S. H.; Jun, S. *J. Phys. Chem. B* **1999**, *103*, 7743.
(10) Ehrburger-Dolle, F.; Morfin, I.; Geissler, E.; Bley, F.; Livet, F.; Vix-Guterl, C. *Langmuir* **2003**, *19*, 4303.
(11) Vix-Guterl, C.; Boulard, S.; Parmentier, J.; Werckmann, J.; Patarin, J. *Chem. Lett.* **2002**, *10*, 1062.
(12) Zhao, D.; Huo, Q.; Stuky, G. D.; Feng, J.; Melosh, N.; Fredrickson, G. H. *Science* **1998**, *279*, 548.
(13) Campesi, R.; Cuevas, F.; Gadiou, R.; Leroy, E.; Hirscher, M.; Vix-Guterl, C.; Latroche, M. *Carbon* **2008**, *46*, 206.

10.1021/ja101795g

diffraction, and X-ray absorption experiments have been performed to characterize the hydrogen sorption properties of the hybrid material. A thorough comparison between the hydrogen sorption properties of the hybrid material, the carbon precursor, and bulk Pd will be addressed and will clarify the size dependent properties of the Pd clusters.

Experimental Details

The carbon template (CT) was obtained by a replica method of the SBA-15 silica, as described elsewhere.[9−11] The SBA-15 silica was prepared according to the synthesis procedure already presented in the literature.[12] It displays cylindrical pores with a diameter close to 5 nm and a mean wall width of ∼4 nm. Carbon was deposited into the SBA-15 porosity by chemical vapor deposition (CVD) of a mixture of 3 vol % of propylene and argon at 1023 K. The total amount of carbon introduced in the SBA-15 porosity is 37 wt %. To remove the silica template, the mixed material (silica/carbon) was stirred for 4 h in a HF solution (40% volume concentration) before being filtered and washed with distilled water and finally dried at 80 °C overnight. The as-synthesized CT displays a hexagonal arrangement of carbon nanorods (4.5 nm) and a very well organized mesoporosity. The total mesoporous volume is 1.1 m^3/g with a narrow pore size distribution of around 5 nm.

To generate in situ Pd nanoparticles (nPd) into the CT porosity, a chemical wetting procedure was used, as described elsewhere.[13,14] A solution of tetrachloropalladous acid (H_2PdCl_4) was prepared by mixing 0.3353 g of $PdCl_2$ (Alfa Caesar, purity 99.9%) into 20 mL of 10% vol HCl aqueous solution under stirring at 300 K until complete dissolution. The CT in powder form was then impregnated twice with the tetrachloropalladinic acid solution for a final Pd concentration of around 20 wt %. The mixture of powder and solution was stirred for 3 h and dried in air at 330 K. The $PdCl_4^{2-}$ ions were reduced by heating the impregnated CT in a Ar/H_2 flow (0.5 L min^{-1}) at 573 K for 6 h. The sample was then outgassed under secondary vacuum for 11 h at 573 K.

The chemical composition of the impregnated material has been determined by an inductively coupled plasma optical emission spectrometer (ICP-OES). The measured Pd content is 17.2 wt %, close to the nominal composition. The hybrid material will further be named CT/nPd.

Microstructural analyses were performed by transmission electron microscopy (TEM-Tecnai F20 with a field emission gun of 200 kV, punctual resolution of 0.24 nm, and energy filtering GIF), and the chemical composition was determined by energy dispersion spectroscopy (EDS).

The textural properties were determined from nitrogen adsorption/desorption isotherms measured with a Micromeritics ASAP 2020 instrument. The specific surface area was obtained by the Brunauer−Emmett−Teller (BET) method. The total pore volume was computed from the amount of gas adsorbed at $p/p_0 = 0.99$, and the micropores volume was calculated using the Dubinin−Radushkevich equation in the relative pressure range 10^{-4}−10^{-2}.

Structural characterizations were performed by X-ray diffraction (XRD) using a Bruker D8 Advance instrument (Cu Kα, Bragg−Brentano geometry). To characterize the crystallographic changes induced by hydrogen absorption in CT/nPd, in situ XRD measurements were performed by stepwise increase of hydrogen pressures at ambient temperature. The sample was initially evacuated under primary vacuum, and hydrogen pressure was incremented to 10 kPa. As reference, in situ XRD measurements have been performed on bulk Pd (bPd) powder (<100 μm) under comparable conditions.

Hydrogen sorption properties were determined by measuring the pressure−composition isotherms (PCI) at 77 and 298 K to 9 MPa hydrogen pressure. The PCI curves were recorded using a manual volumetric device (Sievert's method) equipped with calibrated and thermostated volumes and pressure gauges. The samples were enclosed in a stainless steel sample holder closed with a metal seal. Before any sorption measurements, the samples were outgassed under primary vacuum at 473 K for 10 h. The sample holder is immersed in a liquid N_2 Dewar at 77 K or in a thermostated water bath maintained at 298 K, and high purity hydrogen (6 N) is introduced step by step up to 9 MPa. The pressure variations due to both gas cooling and hydrogen sorption are measured after reaching thermodynamic equilibrium, usually in the range of minutes. The real equation of state for hydrogen gas was used from the program GASPAK V3.32.[15] The PCI curves were measured twice (i.e., two full adsorption−desorption cycles) to check the hysteresis effect and the measurement repeatability. One additional PCI curve at room temperature and H_2 pressure up to 0.4 MPa has been measured with the help of an automated volumetric instrument (PCTPro) to confirm the manually recorded isotherm for CT/nPd. Good agreement is noticed between the two types of measurements. All capacities reported here in wt % are determined with respect to the hydrogen loaded material after correction of the sample weight loss by outgassing. Sample volume correction is derived from density measurement obtained with a helium AccuPyc 1330 Micromeritics pycnometer. By use of this method, the measured densities of CT and CT/nPd are 1.8 ± 0.2 and 2.5 ± 0.1 g cm^{-3}, respectively.

The local structure of the nPd was investigated by X-ray absorption spectroscopy (XAS) in transmission mode on SAMBA beamline at the SOLEIL synchrotron. The X-ray absorption spectra at the K edge of Pd were measured under vacuum at 77 and 298 K and under hydrogen atmosphere (80 kPa) at 298 K. Bulk Pd powder (<100 μm) was also measured under similar conditions and used as reference. The powder samples were mixed with a polymer (PTFE) to ensure the mechanical cohesion. The measurements were performed in a special cell connected to a gas sorption device that allows careful control of the hydrogen pressure.[16] The XAS data treatment and the EXAFS modeling and fit were performed by the help of the MAX program package.[17] The FEFF8 program was used to obtain the theoretical phase shifts and amplitudes of the Pd−Pd(O) shells.[18] The photoelectron mean free path was determined empirically. The refined parameters are the coordination number (N), the Debye−Waller factor (σ^2), the distance between the shells (R), and the energy shift (ΔE_0). A single Pd−Pd shell model was successfully used for almost all spectra, excluding the nPd under vacuum at 298 K, where a two-shell (Pd−O and Pd−Pd) model has to be taken into account because of the presence of oxygen. The energy shift ΔE_0 was close to zero for all refinements.

Neutron powder diffraction (NPD) experiments were performed on D1B instrument at the Institute Laue Langevin. This instrument can provide high neutron flux with a wavelength of 2.52 Å and is suitable for in situ study under different gas pressure and temperature conditions. In situ neutron diffraction was measured during the thermal D_2 desorption with the help of a special sample holder. The silica sample holder can be used in a wide range of temperature and pressure conditions. Deuterium isotope has been chosen instead of hydrogen because of its lower incoherent scattering cross section. Bulk Pd powder and pristine CT were also measured under comparable gas pressure and temperature conditions and used as references. The thermal desorption spectra (TDS) were recorded simultaneously to neutron diffraction patterns as the total pressure under dynamic high vacuum while applying a constant temperature

---

(14) Campesi, R.; Cuevas, F.; Leroy, E.; Hirscher, M.; Gadiou, R.; Vix-Guterl, C.; Latroche, M. *Microporous Mesoporous Mater.* **2009**, *117*, 511.

(15) Lemmon, E. W.; Peskin, A. P.; McLinden, M. O.; Friend, D. G. *NIST12 Thermodynamic and Transport Properties of Pure Fluids*, version 5.0; NIST: Gaithersburg, MD, 2000.

(16) Paul-Boncour, V.; Joubert, J.-M.; Latroche, M.; Percheron-Guégan, A. *J. Alloys Compd.* **2002**, *330−332*, 246.

(17) Michalowicz, A.; Moscovici, J.; Muller-Bouvet, D.; Provost, K. *J. Phys.: Conf. Ser.* **2009**, *190*, 012034.

(18) Ankudinov, A. L.; Ravel, B.; Rehr, J. J.; Conradson, S. D. *Phys. Rev. B* **1998**, *58*, 7565.

Table 1. Textural and Hydrogen Sorption Properties of CT and CT/nPd[a]

properties	CT	CT/nPd
BET surface area (m^2/g)	960 ± 10	660 ± 7 (795)
$V_{0.99}$ (cm^3/g)	1.10 ± 0.1	0.75 ± 0.1 (0.90)
$V_{\mu p}$ (cm^3/g)	0.2 ± 0.1	0.3 ± 0.1 (0.3)
excess hydrogen capacity, 4 MPa, 77 K (wt %)	1.80 ± 0.1	1.45 ± 0.1
excess hydrogen capacity, 4 MPa, 298 K (wt %)	0.13 ± 0.02	0.23 ± 0.02

[a] The values of BET surface area, total porous volume ($V_{0.99}$), and microporous volume ($V_{\mu p}$) are given by gram of sample and in parentheses by gram of carbon.

rate of 0.42 K min^{-1} from 22 to 310 K. The samples were previously loaded at room temperature with D_2 gas with the help of a Sieverts apparatus. The CT and CT/nPd were loaded with the same amount of dosed D_2. The bulk deuteride ($bPdD_{0.6}$) was formed at room temperature by deuterium uptake at 0.05 MPa pressure. Afterward, all samples have been cooled under D_2 atmosphere to 22 K. The remaining amount of gas that has been not adsorbed (absorbed) by the sample was removed by pumping.

Results

1. Microstructural, Textural, and Hydrogen Sorption Properties. The structural and microstructural investigations of CT/nPd have proven that the hybrid material is formed by Pd nanoparticles (nPd) well dispersed in the porous structure of the CT, as recently published by Campesi et al.[13] The nPd adopts a fcc structure with the lattice parameter $a = 3.93 \pm 0.02$ Å comparable to the cubic crystal structure of bulk Pd (bPd).[19] The mean size of the nPd is 2.5 ± 0.5 nm, as determined by both XRD (Scherrer's formula) and TEM analysis. The textural properties of CT and CT/nPd at 77K are listed in Table 1. The decrease of specific surface area and total porous volume of CT/nPd hybrid compared to the precursor CT can be explained by the increase of the total weight (by 17.2%) together with the blocking of accessible pores by insertion of nPd. The micropore volume does not change significantely after the formation of the nPd, proving that nanoparticles are located in the mesopores of the CT material. The change of textural properties has consequences on the hydrogen storage properties, as discussed later.

The hydrogen sorption properties have been determined by measuring the PCI curves at 77 and 298 K (Figure 1). The Gibbs excess hydrogen adsorption capacities of CT and CT/nPd at 77 and 298 K at 4 MPa are given in Table 1. At 77 K, the excess sorption isotherms of both samples display a type I trend typical for monolayer adsorption on porous materials (Figure 1a). The hydrogen capacity of pristine CT is in good agreement with previously reported values for porous materials with similar surface area.[20,21] At room temperature, the PCI curve of CT (Figure 1b) displays a linear shape typical for diluted monolayer adsorption (Henry type), as commonly reported for porous materials at this temperature. The isotherm of CT/nPd shows a steep rise at low pressure that can be attributed to the hydrogenation of nPd clusters and formation of $nPdH_x$ hydride. For higher pressure, a linear increase of the hydrogen uptake is observed that is ascribed to H_2 physisorption on the carbon porosity. The desorption branch of the PCI curve of CT/nPd shows an irreversible character at very low pressure.

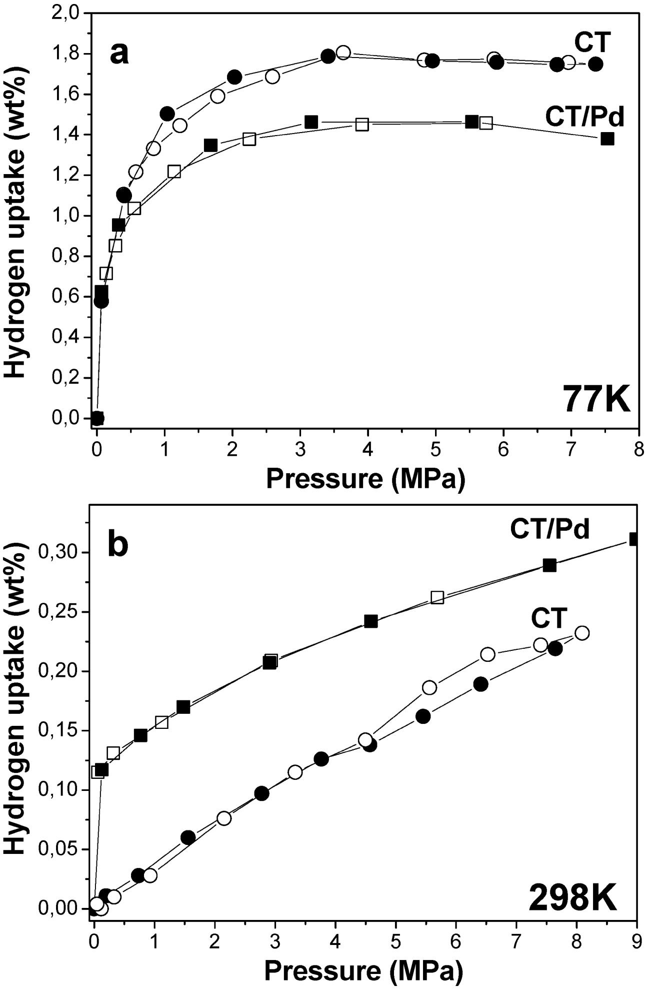

Figure 1. PCI curves of CT (circle) and CT/nPd (square) recorded at 77 K (a) and 298 K (b). Full and empty symbols stand for ad/absorption and desorption, respectively.

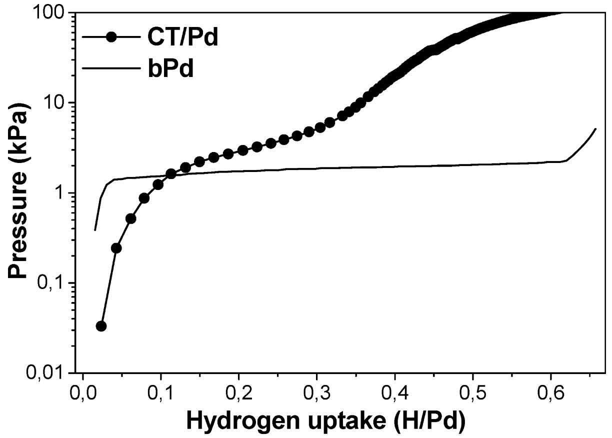

Figure 2. Absorption PCI of CT/nPd at 298 K measured to 100 kPa (full circles). For comparison, the absorption PCI of bPd is also plotted (line).

Hydrogenation of nPd has been measured at low pressure and room temperature (where the hydrogen adsorption by CT is negligible) and compared to bPd (Figure 2). Under hydrogen pressure below 1 kPa, the nPd forms a solid solution of hydrogen in Pd (α phase) followed by the formation of the hydride $nPdH_x$ (β phase), as verified by the presence of a sloping plateau pressure. The formation of the hydride $nPdH_x$ is complete at 5

---

(19) Bidwell, L. R.; Speiser, R. *Acta Crystallogr.* **1964**, *17*, 1473.
(20) Thomas, M. K. *Catal. Today* **2007**, *120*, 389.
(21) Ströbel, R.; Garche, J.; Moseley, P. T.; Jörissen, L.; Wolf, G. *J. Power Sources* **2006**, *159*, 781.

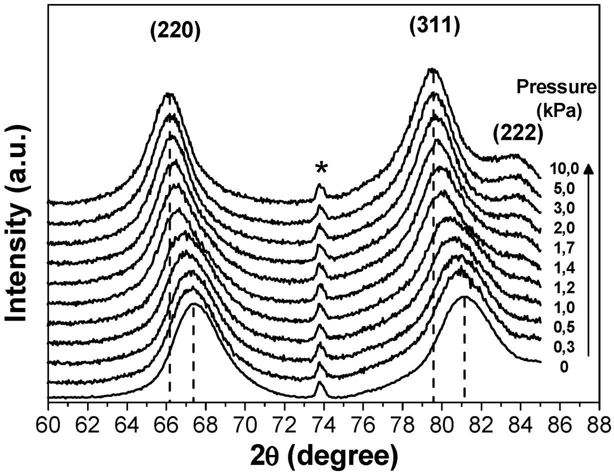

Figure 3. In situ XRD patterns during hydrogenation of nPd at 290 K. The applied H_2 pressure is indicated. The diffraction peak at 74° (*) belongs to the sample holder.

kPa hydrogen pressure. The plateau pressure of nPd appears in the same pressure region as bPd, although it is sloped compared to bPd. Moreover, the length of the plateau pressure of nPd is reduced compared to bPd.

2. In Situ Hydrogen Sorption. To give a comprehensive picture of the hydrogen sorption mechanism in CT/nPd hybrid, in situ hydrogen sorption investigations have been performed using XRD, XAS, and NPD. Systematic comparisons with bPd and pristine CT have been performed under similar pressure and temperature conditions.

The hydrogenation of the nPd of the hybrid material was monitored by in situ XRD during stepwise increase of H_2 pressure to 10 kPa at 290 K (Figure 3). The most intense (111) and (200) diffraction peaks of nPd overlap with a broad diffraction contribution from the CT.[13] For the sake of the clarity, the angular domain between 60° and 85° was chosen for in situ measurements because it contains two distinct diffraction peaks, indexed as (220) and (311) in the fcc structure, and no carbon contribution. Moreover, in this angular domain an extra diffraction peak belonging to the sample holder appears at around 74° and serves as a reference. The diffraction peaks of nPd shift to lower angle with increasing H_2 pressure, in agreement with the volume expansion due to the hydrogenation. Below 1 kPa, a small shift of the Bragg peaks is noticed and corresponds to the formation of the α phase (fcc). Higher H_2 pressure (above 1.2 kPa) induces both a shift of the Bragg peak and an increase of the peak height. This indicates the start of the formation of the hydride $nPdH_x$ (the β phase). Because of the strong overlap between the diffraction peaks of α and β phases, a clear determination of the $\alpha-\beta$ miscibility limits cannot be done by this method. For pressure higher than 5 kPa, the formation of the $nPdH_x$ hydride is completed. These results are in good agreement with the isotherm of nPd measured at room temperature (Figure 2).

Since the thermodynamics of hydrogenation of bPd is well documented,[22] a comparison between in situ XRD measurements of hydrogenation of nPd and bPd (powder) was performed under similar conditions. The (220) diffraction peak of nPd (at 0 kPa) and $nPdH_x$ (at 10 kPa) from Figure 3 are replotted in Figure 4 and compared to those from bPd and its hydride $bPdH_{0.6}$. The peak shift due to the formation of the hydride is larger in the case of bPd than nPd, indicating different volume expansion. The lattice parameters of nPd, $nPdH_x$, bPd, and $bPdH_{0.6}$ and the relative lattice expansion due to hydrogenation are listed in Table 2 together with the intensity (integrated area after background correction) and full width at half-maximum (fwhm) of the (220) peak (from Figure 4). The lattice expansion induced by hydrogenation is larger in bPd compared to nPd. The peak intensities of both hydride phases are slightly larger than the corresponding metal states. However, the variation of the fwhm is different; the $nPdH_x$ shows a narrowing of the fwhm relative to nPd, while the fwhm increases from bPd to $bPdH_{0.6}$. This feature of nPd is completely reversible with hydrogenation/dehydrogenation cycling.

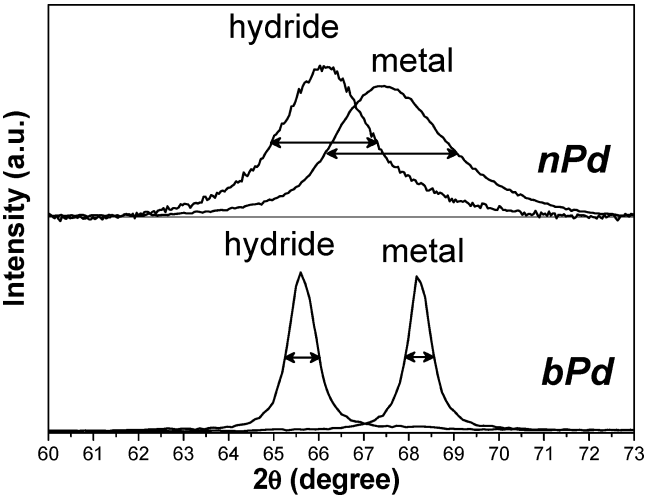

Figure 4. Comparison of the (220) diffraction peak for the metal and hydride phases of nPd (top) and bPd (bottom). The diffraction patterns of nPd correspond to those measured at 0 and 10 kPa hydrogen pressure in Figure 3.

Table 2. Structural Properties of nPd, $nPdH_x$, bPd, $bPdH_{0.6}$: Lattice Parameter (*a*), Relative Lattice Expansion ($\Delta a/a$), Integrated Area after Background Correction (I), and Full Width at Half Maximum (fwhm) of the (220) Bragg Peak[a]

sample	*a* (Å)	Δ*a*/*a* (%)	*I* (220) (a.u.)	fwhm (220) (deg)
nPd	3.93 ± 0.02		1	2.85
$nPdH_x$	4.00 ± 0.02	1.8	1.07	2.19
bPd	3.884 ± 0.005		1	0.53
$bPdH_{0.6}$	4.025 ± 0.005	3.6	1.17	0.70

[a] The integrated area of the hydride phases are normalized to the corresponding intensity of the metallic diffraction peak.

In situ XAS investigations have been performed at the Pd K edge to study the nPd and bPd in both metallic (under vacuum) and hydride states (under 80 kPa hydrogen pressure) at 298 K. The EXAFS spectra and the module of the Fourier transform (FT) are shown in Figures 5 and 6 for nPd and bPd, respectively. The FT peaks of the hydride phase are shifted to larger distances compared to the metallic state, irrespective of the nature of Pd (bulk and nanoparticles). A larger increase of the distance is noticed for $bPdH_{0.6}$ than for the $nPdH_x$. The intensities of all FT peaks decrease from metal to hydride state in the case of bPd, whereas an opposite effect occurs for nPd. The FT of the metallic nPd (Figure 5) shows that near the main peak due to Pd−Pd backscattering, a smaller peak is present at lower distance and can be accounted by the Pd−O backscattering, in good agreement with previous EXAFS study of reduction and

---

(22) Frieske, H.; Wicke, E. *Ber. Bunsen-Ges. Phys. Chem.* **1973**, *77*, 48.

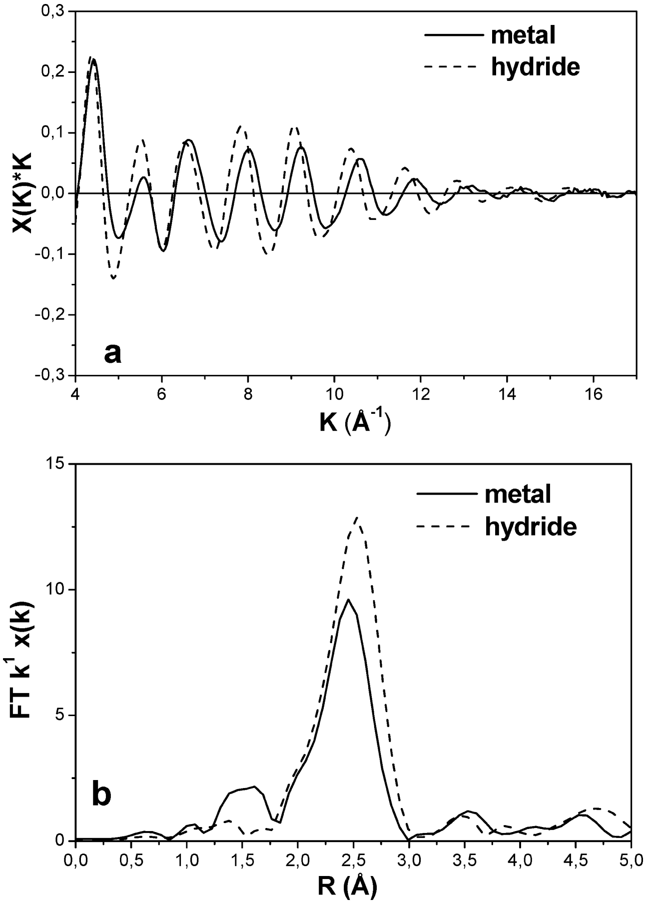

Figure 5. Experimental EXAFS spectra (a) and corresponding module of the Fourier transform (b) of nPd in metallic (line) and hydride (dashed line) states at 298 K.

reoxidation of Pd nanoparticles.[23,24] In contrast, the FT of the corresponding hydride nPdH$_x$ has only one peak due to the Pd−Pd backscattering with enlarged amplitude compared to metal. The Pd−O backscattering peak disappears upon hydrogenation, indicating that a reduction of the oxide layer occurs while exposure to hydrogen. The oxidation state of nPd was also checked by probing a completely different part of the same sample at 77 K. The low temperature reduces the thermal contribution of the Debye−Waller factor, and therefore, the structural model can be undoubtedly determined. Surprisingly, the FT at 77 K has only a single peak due to the first Pd−Pd shell, indicating that this part of the sample is oxygen-free. Moreover, a comparison of the related XANES spectra (from the two different positions of the sample) clearly proves that the part of the sample investigated at 298 K is slightly oxidized, since the ratio of the first two oscillations after the absorption edge is changed respective to the 77 K spectrum (Figure 1 of the Supporting Information). This suggests that the as-prepared sample is not homogeneous with respect to oxygen. Some parts are slightly oxidized and subsequently reduced in hydrogen atmosphere. This might indicate that the oxygen is chemisorbed at the surface of nPd. This is not the case for bPd, which shows a single peak in the FT for both metal and hydride (Figure 6).

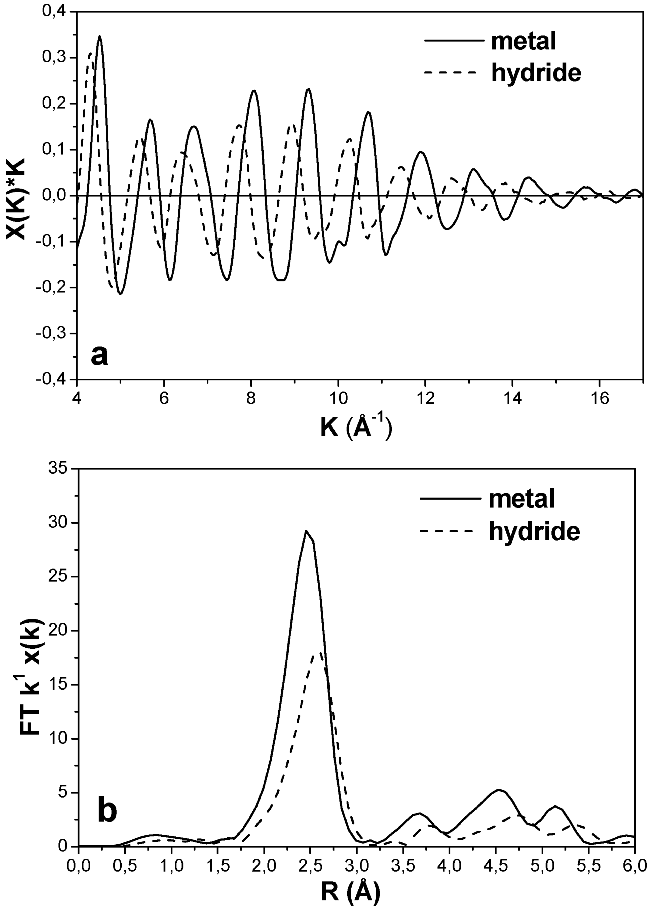

Figure 6. Experimental EXAFS spectra (a) and corresponding module of the Fourier transform (b) of bPd in metallic (line) and hydride (dashed line) states at 298 K.

Table 3. Refined Parameters of the EXAFS Spectra of nPd, nPdH$_x$, and bPd, bPdH$_{0.6}$ Samples: Distance of the Nearest Neighbors (*R*), Coordination Number (*N*), Debye−Waller Factor (σ^2), and Confidence Factor of the Fit (QF)

sample	*T* (K)	shell	*R* (Å)	*N*	σ^2 (Å^2)	QF
nPd	77	Pd−Pd	2.75 ± 0.01	7.5 ± 0.6	0.004 ± 0.001	0.1
	298	Pd−Pd	2.74 ± 0.01	6.4 ± 0.8	0.008 ± 0.001	0.1
	298	Pd−O	1.97 ± 0.01	1.5 ± 0.3	0.004 ± 0.002	
nPdH$_x$	298	Pd−Pd	2.79 ± 0.01	9.0 ± 0.8	0.008 ± 0.001	0.1
bPd	77	Pd−Pd	2.74 ± 0.01	12 (fixed)	0.003 ± 0.001	0.1
	298	Pd−Pd	2.74 ± 0.01	12 (fixed)	0.006 ± 0.002	0.5
bPdH$_{0.6}$	298	Pd−Pd	2.84 ± 0.01	11.5 ± 0.9	0.008 ± 0.001	0.1

The first atomic shell was filtered between 1 and 3 Å and refined (Figures 2 and 3 of the Supporting Information) with one Pd−Pd shell for bPd, bPdH$_{0.6}$, nPd (at 77 K), and nPdH$_x$ and with two shells ($R_{\text{Pd−Pd}} = 2.74$ Å and $R_{\text{Pd−O}} = 1.96$ Å) in the case of nPd (at 298 K). The refined structural parameters are listed in Table 3, showing the distance of the nearest neighbors (*R*), the coordination number (*N*), and the Debye−Waller factor (σ^2) together with the confidence factor of the refinement (QF).

The distances of the nearest Pd−Pd neighbors, as determined by EXAFS analysis, show good agreement with XRD data for bPd and bPdH$_{0.6}$ ($a/\sqrt{2}$ in Table 2), whereas it is 0.04 Å smaller for nPd (2.74 Å vs 2.78 Å) and nPdH$_x$ (2.79 Å vs 2.83 Å). This systematic difference between the nearest Pd−Pd distances determined by EXAFS and XRD in the case of nanoparticles might be explained by surface strain effects affecting this

---

(23) Caravati, M.; Meier, D. M.; Grundwaldt, J.-D.; Baiker, A. *J. Catal.* **2006**, *240*, 136.

(24) Grunwaldt, J.-D.; Caravati, M.; Baiker, A. *J. Phys. Chem B* **2006**, *110*, 25586.

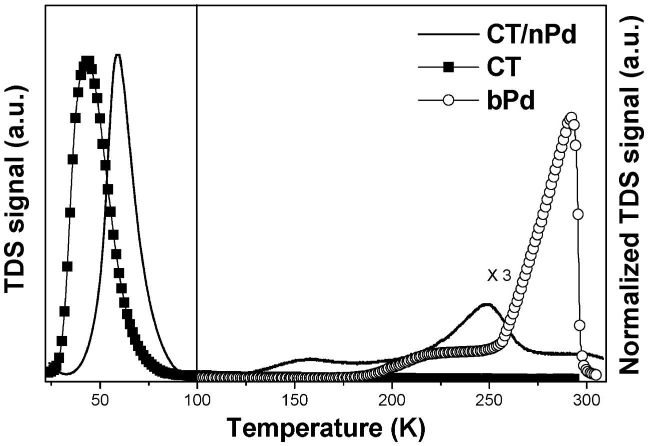

Figure 7. Comparison of the TDS signals from CT/nPd (line), CT (full square), and bPd (empty circle) recorded between 22 and 310 K with a constant temperature rate of 0.42 K min^{-1}. For the sake of clarity, above 100 K, both CT/nPd curve (line) and bPd spectra (empty circle) were normalized to the weight of Pd and then multiplied by 3.

parameter. The hydrogenation induces an expansion of $R_{\mathrm{Pd-Pd}}$ distances in both hydrides; however, this is larger in bPd than in nPd, in agreement with in situ XRD results (Table 2).

The Pd coordination number of the first shell in oxygen-free samples is reduced from 12 in bPd (fcc structure) to 7.5 and 9.0 in the case of nPd and nPdH$_x$, respectively, in agreement with the small particle size.[25] In the case of slightly oxidized nPd (at 298 K), N decreases to 6.4 compared to 7.5 for oxygen-free nPd (at 77 K). This feature is commonly observed during oxidation and reduction of metallic particles.[26]

The Debye−Waller factor increases from 77 to 298 K because of amplified thermal vibrations. It also rises from bPd to bPdH$_{0.6}$, in agreement with the introduction of defects by hydrogenation, as already observed by in situ XRD and in previous EXAFS studies.[27,28] The Debye−Waller factor of the first Pd−Pd layer remains unchanged for nPd and nPdH$_x$ at 298 K.

Several FT peaks are observed at distances larger than 3 Å and can be attributed to simple and multiple-scattering on further Pd atoms (Figures 5 and 6). These contributions were simulated for bPd and bPdH$_x$ with the help of FEFF8 with additional Debye−Waller factors those values increase with distance. The simulation of the EXAFS spectra by taking into account the presence of the interstitial H atoms in the metallic structure has proven no additional multiple scattering effects compared to Pd−Pd backscattering.

Thermal desorption of deuterium from deuterated CT/nPd, CT, and bPd has been studied simultaneously with in situ neutron powder diffraction. A comparison between the three TDS spectra is shown in Figure 7. The desorption of physisorbed D$_2$ in CT/nPd occurs at higher temperature than that of CT. The deuterium desorption from the fully deuterated nPd has a double-peak shape like that of bPd, in good agreement with the previous results from bPd.[29] However, deuterium is desorbed at lower temperature in nPd than in bPd.

The in situ NPD of CT/nPd during D$_2$ desorption (not shown here) shows only broad diffraction peaks arising mainly from the CT component, in agreement with its weak structural order, but no diffraction peaks from nPd are observed. This is due to the low amount of nPd (17 wt %), its small particle size, and the very close scattering lengths of Pd and C (0.6 × 10^{-12} and 0.665 × 10^{-12} cm for C and Pd, respectively[30]). The neutron diffraction patterns from CT are very similar to those of CT/nPd, since mainly CT is contributing to diffraction. In both cases, obvious differences between the diffraction patterns recorded at full D$_2$ loading and complete unloading (Figure 8a) are noticed. The pattern difference clearly shows the existence of a peak at around $2\theta = 45°$, or $Q \approx 1.9$ Å^{-1} ($\lambda = 2.52$ Å). Moreover, the difference between the diffraction patterns evolves with temperature (Figure 8b). The position of the peak does not change with temperature, but its area decreases with temperature. The integrated area of this peak (after background correction and normalization relative to the highest value) is plotted as a function of temperature in Figure 8c together with the thermal evolution of the D$_2$ coverage, as extracted from the TDS spectrum. A good agreement is noticed, which indicates that the difference peak can be directly related to the surface coverage of D$_2$ molecules on the porous material. In a similar way, the difference of diffraction patterns of CT/nPd shows the presence of a peak at $Q \approx 1.9$ Å^{-1}, whose area and temperature evolution correlate with the thermal progress of the D$_2$ coverage, as extracted from TDS signal (not shown here).

Discussion

The present hybrid material CT/nPd is formed by ultrasmall Pd nanoparticles (2.5 nm) embedded in the mesopores of an ordered carbon template. The insertion of nPd in the porosity of the CT reduces the textural properties of hybrid material (Table 1). This decrease supports the observed loss of excess hydrogen sorption at 77 K in CT/nPd relative to CT (Figure 1a). The H$_2$ sorption mechanism on CT/nPd at low temperature is governed by molecular physisorption on the surface of the porous material. At ambient temperature, the excess hydrogen capacities of both CT and CT/nPd are small (below 0.5 wt %). The CT/nPd shows higher capacity than CT (Figure 1b and Table 1), and this can be explained by the hydrogenation of nPd and the formation of nPdH$_x$ that is kinetically hindered at 77 K. For pressure up to 0.1 MPa, the adsorption of H$_2$ on CT is almost negligible (Figure 1b). Therefore, the hydrogen uptake of CT/nPd measured at 0.1 MPa can be almost entirely attributed to the formation of nPdH$_x$. Under this assumption, the calculated H/Pd ratio for nPdH$_x$ is approximately 0.6 (details of the calculation are given in the Supporting Information), a value higher than the commonly reported 0.3−0.4 for the hydride formation of Pd nanoparticles under similar temperature and pressure conditions.[31−35] A cooperative effect between the metal nanoparticles and the porous host might take place leading to

---

(25) Frenkel, A. I.; Hills, C. W.; Nuzzo, R. G. *J. Phys. Chem. B* **2001**, *105*, 12689.

(26) Newton, M.; Belver-Coldeira, C.; Matrinez-Arias, A.; Fernandez-Garcia, M. *Nat. Mater.* **2007**, *6*, 528.

(27) Rose, A.; Maniguet, S.; Mathew, R. J.; Slater, C.; Yao, J.; Russell, A. E. *Phys. Chem. Chem. Phys.* **2003**, *5*, 3220.

(28) Davis, R. J.; Landry, S. M.; Horsley, J. A.; Boudart, M. *Phys. Rev. B* **1989**, *39*, 10580.

(29) Stern, A.; Resnik, A.; Shaltiel, D. *J. Phys. F: Met. Phys.* **1984**, *14*, 1625.

(30) Bacon, G. E. *Neutron Diffraction*, 3rd ed.; Clarendon Press: Oxford, U.K., 1975.

(31) Zütell, A.; Nützenadel, Ch.; Schmid, G.; Emmenegger, Ch.; Sudan, P.; Schlapbach, L. *Appl. Surf. Sci.* **2000**, *162−163*, 571.

(32) Narehood, D. G.; Kishore, S.; Goto, H.; Adair, J. H.; Nelson, J. A.; Gutierrez, H. R.; Eklund, P. C. *Int. J. Hydrogen Energy* **2009**, *34*, 952.

(33) Pundt, A.; Kirchheim, R. *Annu. Rev. Mater. Res.* **2006**, *36*, 555.

(34) Zütell, A.; Nützenadel, Ch.; Schmid, G.; Chartouni, D.; Schlapbach, L. *J. Alloys Compd.* **1999**, *293−295*, 472.

(35) Suleiman, M.; Faupel, J.; Borchers, C.; Krebs, H.-U.; Kirchheim, R.; Pundt, A. *J. Alloys Compd.* **2005**, *404−406*, 523.

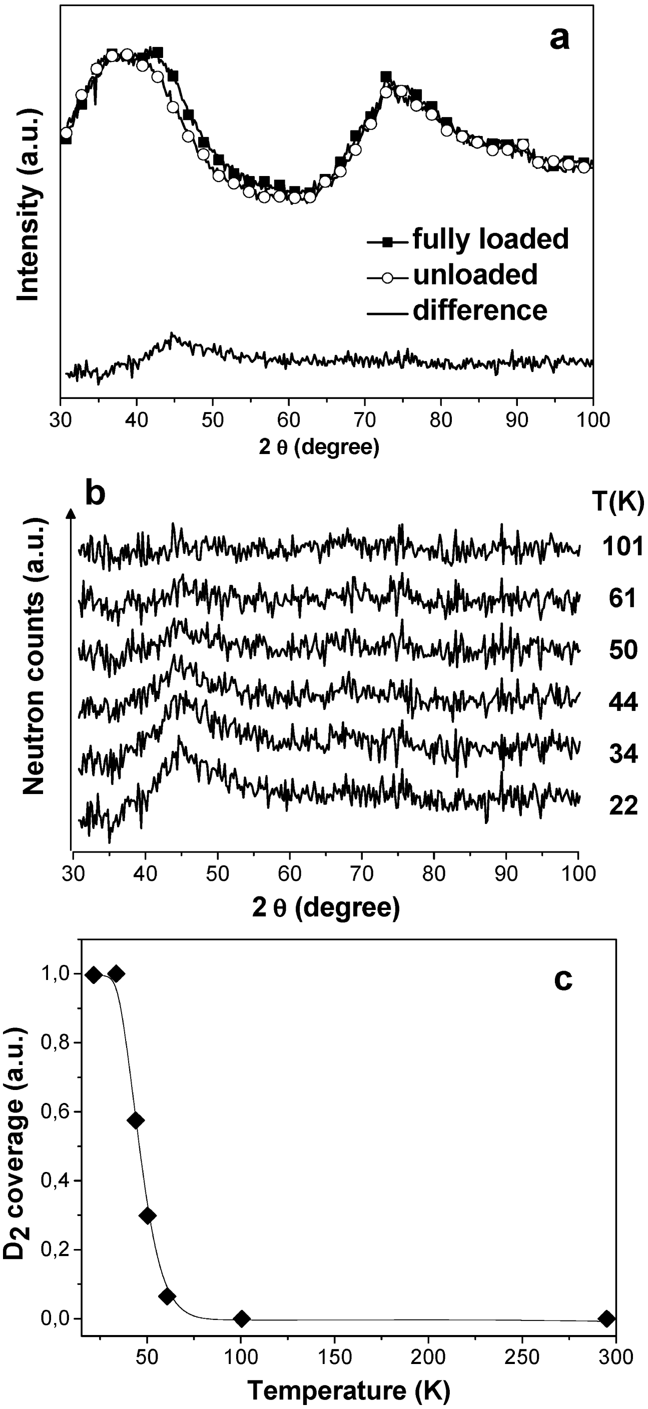

Figure 8. Neutron diffraction patterns of the fully D_2 loaded (22 K) and completely unloaded CT (298 K) together with the difference pattern (a), the thermal evolution of the difference pattern (b), and the thermal evolution of the D_2 coverage as measured by TDS (solid line) and the integral of the difference neutron diffraction patterns (solid square) (c).

an enhancement in the hydrogen uptake, as already proposed earlier.[13,36−38] From the present data, it cannot be concluded that a hydrogen spillover effect occurs, since no evidence for hydrogen bonding in the CT material was proven. Nevertheless, the observed enhancement of capacity is of minor importance compared to a previous report[38] and does not lead to significant improvement of the storage properties.

The hydrogenation isotherms recorded at low pressure and 298 K for nPd and bPd (Figure 2) show that thermodynamic changes introduced by particle downsizing are not encountered. The pressure plateaus of both nPd and bPd are in the same range, although the plateau of nPd is slightly sloped. The origin of the sloped pressure plateau is still an open question and has been previously accounted for by a broad size distribution of cluster sizes or mechanical stress induced by the stabilizing matrix.[33,35] In the present case, the size distribution of nPd is narrow (1.0−3.5 nm) as determined by TEM, which might indicate different origin of the sloping plateau. Moreover, the maximum hydrogen solubility in the α phase increases and the minimum solubility in the β phase decreases in nPd relative to bPd. Subsequently, the $\alpha-\beta$ miscibility region in nPd (0.05−0.3 H/Pd) is lower than in bulk Pd (0.025−0.65 H/Pd), in good agreement with previous results on small Pd clusters.[33] Therefore, the maximum amount of hydrogen absorbed in Pd nanoparticles is lower than in bulk.

Results from in situ XRD investigations during hydrogenation of nPd (Figure 3) are in good agreement with the isotherm measurement at 298 K (Figure 2). The hydrogenation and formation of the α and β phases in nPd occur at the same pressure for both methods, confirming the validity of in situ measurements. The advantage of in situ XRD is related to the structural information that can be obtained on the $\alpha-\beta$ phase transition in nPd.

In situ XRD reveals important differences between nPd and bPd upon hydrogenation (Figure 4 and Table 2). The lattice parameter of metallic nPd is slightly larger than that of bPd and is in good agreement with previously published values.[19] This dilation has been already reported for very small Pd nanoparticles (2−3 nm).[32,35] Upon hydrogenation, the relative lattice expansion $\Delta a/a$ is larger in bPd compared to nPd (Table 2), pointing to a larger volume expansion introduced by hydrogenation in bPd. This difference can be explained by a lower hydrogen content than can be accommodated in the nPd compared to bPd, in agreement with the low pressure isotherm measurements at 298 K (Figure 2) and previous studies.[31−34]

Another important difference between nPd and bPd is related to the change of the fwhm of the (220) Bragg peak from metal to hydride (Figure 4 and Table 2). In the case of bPd, both the peak intensity and the fwhm slightly increase from metal to hydride. This is due to the formation of a large number of defects by hydrogen insertion in the metal structure. In contrast, the fwhm in the case of nPd narrows and its intensity rises when forming the hydride phase. This feature is unusual and might be related to an atomic rearrangement of clusters upon hydrogen uptake.

Similar XRD results have been previously reported by Kaszkur[39] for 5.3 nm Pd nanoparticles. The increase of diffracted intensity and the narrowing of diffraction peaks have been attributed to an enhancement of crystal ordering in the Pd cluster upon hydrogenation. In contrast with our results, Pundt et al. have previously reported that hydrogenation on quasi-free Pd clusters (5 nm) is accompanied by a drop of the diffracted intensity and an increase of the width of the Bragg peaks.[40] This observation was performed by in situ synchrotron

---

(36) Amorim, C.; Keane, M. A. *J. Colloid Interface Sci.* **2008**, *322*, 196.
(37) Contescu, C. I.; Brown, C. M.; Liu, Y.; Bhat, V. V.; Gallego, N. C. *J. Phys. Chem. C* **2009**, *113*, 5886.
(38) Yang, R. T.; Wang, Y. *J. Am. Chem. Soc.* **2009**, *131*, 4224.
(39) Kaszkur, Z. *J. Appl. Crystallogr.* **2000**, *33*, 1262.
(40) Pundt, A.; Dornheim, M.; Guerdane, M.; Teichler, H.; Ehrenberg, H.; Reetz, M. T.; Jisrawi, N. M. *Eur. Phys. J. D* **2002**, *19*, 333.

XRD measurements. Using molecular dynamics simulations, the authors claimed that the XRD results can be explained by a cubic to icosahedral transition in the Pd clusters upon hydrogenation.

The present and previous XRD studies on hydrogenation of Pd nanoparticles show contradictory results. Nevertheless, it is clear that short-range atomic reordering in Pd nanoparticles occurs upon hydrogenation. In situ EXAFS measurements can elucidate the nature of these structural modifications.

An analysis of EXAFS spectra recorded on oxygen-free samples indicates a decrease of coordination number from bPd (12) to nPd (7.5) (Table 3). This can be understood by an increased number of dangling bonds due to the large fraction of surface atoms in small clusters, in agreement with conclusions from previous EXAFS studies on small metallic clusters.[25−28,41] In a perfect geometrical arrangement (i.e., almost spherical shaped), a fcc cluster can be built as a sequential filling of atomic shells around a central atom. For a fcc cluster with a perfect geometrical arrangement and an average diameter of 2.5 nm, the number of atomic shells around the central atom is around 4 (±1) and the average coordination number is 8.9.[42] The N estimated from EXAFS (7.5) is slightly reduced relative to the theoretical value of 8.9 that could be explained by a disorder effect in real nanoparticles. The coordination number increases from metal nPd (7.5) to hydride nPdH$_x$ (9.0). This feature is striking and can be related to a rearrangement of clusters upon hydrogenation, as suggested by the present in situ XRD results.

A similar change in coordination number has been observed previously for Pd nanoparticles during CO/NO cycling (CO gas flushing followed by NO).[26] The authors have claimed that the increase of N could be explained by either a resintering of particles or a morphological variation from a flat toward a hemispherical particle shape. In the present case, the increase of N by sintering during hydrogenation can be refuted because the nanoparticles are well dispersed within the mesopores of CT, which serves as mechanical stabilizer against coalescence. Moreover, the mobility of Pd atoms at room temperature is limited. The second explanation that is based on a transition from flat to hemispherical shape particles is also unlikely to happen in the present case. Usually, metal nanoparticles have a spherical shape to reduce the total surface energy, also confirmed by the present and previous microscopic studies.[13,14,32,36]

On the basis of the present in situ XRD and EXAFS measurements, we suggest that the phase transition that occurs upon hydrogenation of nPd is accompanied by a structural transformation from cuboctahedral to icosahedral symmetry. The cuboctahedron is a close-packing fcc structure and can be seen as a fcc polyhedron enclosed by (100) and (111) surfaces. The icosahedral packing has 5-fold symmetry and can be described as slightly distorted tetrahedrally shaped fcc units whose faces are (111) planes sharing a common vertex, as initially proposed by Mackay.[43] The (100) and (111) fcc surfaces have eight and nine nearest neighbors, respectively. The fcc cuboctahedral to icosahedral transition increases the number of (111) surfaces, and consequently, the average coordination number of the first Pd−Pd neighbors increases.[42] The number of atoms in a perfect and complete geometric filling of both cuboctahedral and icosahedral clusters is the same and follows the series of magical numbers: 13, 55, 147, 309, 561, 923, etc.[44] For the present nPd with an average size of 2.5 nm, the total number of atoms in a cluster would be between 309 and 561. Mackay has demonstrated that the cuboctahedral assembly can be transformed into an icosahedron by geometrical rotations and vice versa.[43] Because of the slight distortion of the icosahedron, the geometrical packing density (0.688) is lower than for the close-packing cuboctahedron (0.749). Lower packing density is in agreement with hydrogen insertion and subsequent expansion of lattice volume.

The icosahedral structure of nPdH$_x$ is stabilized by the hydrogen atoms, and the phase transition from cuboctahedron to icosahedron is completely reversible by dehydrogenation, as noticed in the XRD patterns during hydrogenation/dehydrogenation cycling (not shown here). The small size of nPd is responsible for this phase transition, since it is completely absent in bulk system. The 5-fold symmetry is forbidden in bulklike systems because of the absence of translational periodicity.

The spectra of the thermal desorption of D_2 from CT and CT/nPd are shown in Figure 7. The desorption of physisorbed D_2 on the surfaces of both CT and CT/nPd takes place below 100 K (Figure 7). This feature is typical for physisorbed gas molecules at low temperature, a process that is governed by weak van der Waals forces. A comparison of the TDS spectra from CT and CT/nPd below 100 K reveals noticeable differences: the maximum desorption peak from physisorbed D_2 is shifted to higher temperature in the case of CT/nPd compared to the CT. This effect is important and implies higher energetic bonds of D_2 molecules physisorbed on the surface of the hybrid material.

At higher temperature, the thermal desorption spectra of absorbed deuterium in nPd and bPd have a two-peak shape (Figure 7). The first desorption peak (at low temperature) points to the dehydrogenation from the β phase, and the most intensive peak corresponds to D_2 desorption that accompanies the β to α phase transformation.[29] In the present case, the whole TDS spectrum from nPd is shifted to lower temperature compared to bPd. The two desorption peaks from nPd have broader temperature domains (120−280 K) relative to bPd (190−300 K) and therefore are clearly separated. The maximum desorption rate from deuterated nPd, corresponding to the maximum of the main peak, occurs at lower temperature (248 K) relative to bPd (291 K). Additionally, the onset temperature of desorption from the β phase starts at lower temperature in nPdD$_x$ (120 K) than in bPdD$_{0.6}$ (180 K). This indicates that nPd has lower thermal stability compared to bPd for both processes: the dehydrogenation from the β phase and the β to α transformation. Since this technique probes kinetic properties and since thermodynamic changes were not observed by downsizing the Pd particle, this behavior could be related to a shorter diffusion path in nanoparticles compared to bulk Pd.

In the entire temperature range (22−310 K), the D_2 desorption from the CT/nPd hybrid hints at a combination of the TDS features of CT and bPd. However, both desorption processes (from physisorbed and absorbed D_2) have different thermal stability compared to pristine CT and bPd. The presence of Pd nanoparticles embedded in CT might increase the energy of bonds between physisorbed D_2 and carbon matrix, and subsequently the temperature of desorption rises compared to CT. On the other hand, the nanometer size of particles kinetically

---

(41) Mierzwa, B.; Kaszkur, Z.; Moraweck, B.; Pielaszek, J. *J. Alloys Compds.* **1999**, *286*, 93.

(42) Shandiz M. A. *Phys. Lett. A* **2008**, DOI: 10.1016/j.physleta.2008.07.011.

(43) Mackay, A. L. *Acta Crystallogr.* **1961**, *15*, 916.

(44) *Handbook of Metal Physics, Metallic Nanoparticles*; Blackman, J. A., Ed.; Elsevier: Amsterdam, The Netherlands, 2009.

destabilizes the D_2 desorption from nPd deuteride relative to bPd deuteride.

From the TDS spectrum of $nPdD_x$ deuteride the total amount of desorbed deuterium can be determined as the integrated area after background correction between 100 and 310 K. This result can then be compared to the corresponding $bPdD_{0.6}$ deuteride. The latter value was measured experimentally and corresponds to the fully loaded bulk deuteride at 0.05 MPa and room temperature (D/Pd = 0.6). As follows, a value of D/Pd = 0.4 is obtained for $nPdD_x$ deuteride. The hydrogen/deuterium capacity of nPd is lower than that of bPd, in good agreement with the room temperature PCI (Figure 2) and in situ XRD results.

The in situ NPD and thermal desorption measurements prove that the difference between the diffraction patterns of fully loaded and completely unloaded CT (Figure 8) and CT/nPd can be related to the surface coverage of D_2 molecules. A similar conclusion has been proposed previously by Rousell et al.[45] The peaks obtained from the difference between fully loaded and unloaded diffraction diagrams can be linked to the short-range order of the D_2 physisorbed molecules at the surface and to the thermal evolution of the D_2 surface coverage of the porous carbon material.

Conclusions

The hydrogen sorption properties of the CT/nPd hybrid material containing 17 wt % Pd nanoparticles (2.5 nm) have been determined and compared to those of pristine CT and bulk Pd. The CT and CT/nPd have very similar hydrogen sorption mechanism at 77 K, which is governed by physisorption of the hydrogen/deuterium molecules in the porosity of the material. The desorption of adsorbed gas molecules occurs below 100 K and implies more energetic reactions in CT/nPd than in CT, as demonstrated by TDS.

At room temperature, nPd is hydrogenated below 0.1 MPa followed by adsorption of hydrogen molecules on the porosity of hybrid material for higher pressure. The thermodynamics of hydrogenation at room temperature is not modified by downsizing the Pd particles relative to bPd. The plateau pressure of the hydride formation in nPd arises in the same pressure range as for bPd. In situ XRD and absorption isotherm at room temperature together with thermal desorption measurements have shown that the maximum hydrogen content stored in nPd is lowered relative to bPd. The $\alpha-\beta$ miscibility region decreases in nPd (0.05−0.3) compared to bPd (0.025−0.65).

The deuterium desorption from nPd occurs at lower temperature than from bPd, as proven by TDS. Shorter diffusion path in nanosized Pd can explain the improvement of desorption kinetics compared to bulk. In the entire temperature range (22−310 K), the D_2 desorption from the CT/nPd hybrid hints at a combination of the TDS features of pristine CT and bPd. However, both desorption processes (from physisorbed and absorbed D_2) have different thermal stability compared to pristine CT and bPd. The presence of nPd embedded in CT increases the desorption temperature of physisorbed D_2 compared to CT. The nanometer size of Pd particles kinetically destabilizes the D_2 desorption from nPd deuteride relative to bPd deuteride.

These results are gathered and compared in Figure 9, which shows the hydrogen storage capacities of the hybrid and the CT precursor (at 77 and 298 K) and the desorption temperatures of the hybrid, CT, and bulk Pd. If the hydrogen capacity of hybrid is reduced at 77 K compared to the pristine CT, this is reversed at room temperature, where the hybrid has larger capacity. Therefore, the thermal variation of the capacity in the case of the hybrid is smaller than the CT. On the other hand, the difference in the thermal stability between the physisorbed and absorbed hydrogen is smaller for the hybrid relative to the two precursors (CT and bulk Pd), as plotted in Figure 9. This shows the double advantage of the presence of nPd embedded in CT relative to both the hydrogen storage capacity and the two desorption processes (from physisorbed and absorbed hydrogen).

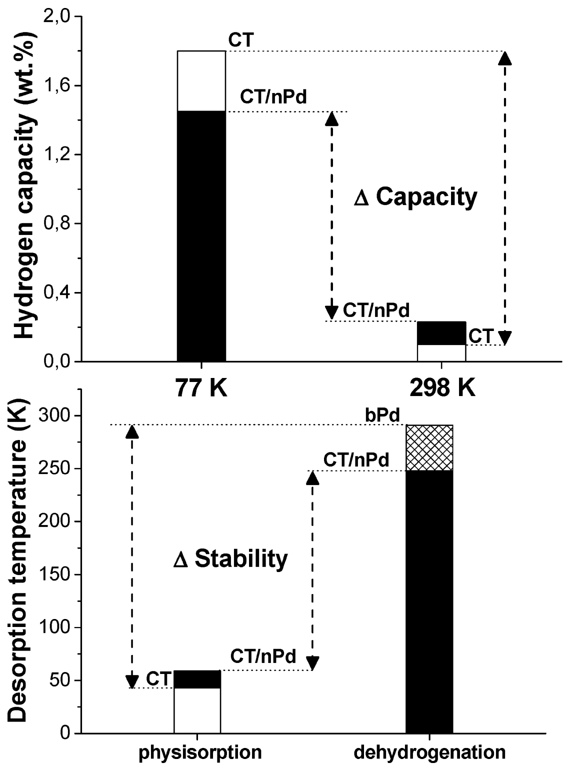

Figure 9. Comparison of the hydrogen storage capacities of the hybrid material CT/nPd and the carbon precursor CT at 77 and 298 K (top). Comparison of the maximum desorption temperatures (and related thermal stability) during desorption of hydrogen for CT/nPd, CT, and bPd (bottom).

In situ XRD and XAS investigations during hydrogenation of nPd have elucidated another size dependent effect on the sorption properties. An atomic rearrangement of clusters during hydrogenation was suggested by in situ XRD on nPd. This behavior was clarified by in situ EXAFS measurements, which indicate that nPd can transform from cuboctahedral to icosahedral structure during hydrogenation. The icosahedral structure is stabilized by hydrogen atoms, and the transition is completely reversible by dehydrogenation. This peculiar transition is related to the small size of Pd nanoparticles, given that it is forbidden in bulk systems because of the nontranslational periodicity of the 5-fold symmetry.

In conclusion, this study has clearly confirmed that downsizing the Pd particle dimensions dramatically changes the interaction with hydrogen relative to the bulk system.

Acknowledgment. The present work has received funding from the French ANR agency through the MATHYSSE project (Contract ANR-07-PANH-007-01). The authors thank Diana Dragoe from

---

(45) Roussel, T.; Pellenq, R. J.-M.; Bienfait, M.; Vix-Guterl, C.; Gadiou, R.; Beguin, F.; Johnson, M. *Langmuir* **2006**, *22*, 4614.

ICMPE, Thiais, France, for ICP-OES measurements, J.-L. Soubeyroux for neutron powder diffraction assistance as local contact on D1B line at ILL (Grenoble, France), J.-P. Gonzales from the SANE Department at ILL for the special neutron diffraction sample holder, S. Belin for valuable help for X-ray absorption spectroscopy on SAMBA beamline at SOLEIL synchrotron (Saint Aubin, France), and Alain Michalowicz from ICMPE, Thiais, France, for precious help with the EXAFS analysis and refinement programs.

Supporting Information Available: Calculation of the H/Pd for Pd nanoparticles from the hydrogen sorption isotherm of CT/nPd hybrid material recorded at room temperature, XANES spectra of Pd nanoparticles embedded in CT from two different positions of the sample, and experimental filtered EXAFS spectra and the module of the Fourier transforms together with the corresponding refined curves for Pd nanoparticles and bulk. This material is available free of charge via the Internet at http://pubs.acs.org.

JA101795G